IAUS300, Nature of prominences and their role in Space Weather
Proceedings IAU Symposium No. S300, 2014
B. Schmieder, J.M. Malherbe & S.T. Wu, eds.

DOI: 00.0000/X000000000000000X

Evolution of interplanetary coronal mass ejections and magnetic clouds in the heliosphere

Pascal Démoulin

Observatoire de Paris, LESIA, UMR 8109 (CNRS), F-92195 Meudon Principal Cedex, France
email: Pascal.Demoulin@obspm.fr

Abstract. Interplanetary Coronal Mass Ejections (ICMEs), and more specifically Magnetic Clouds (MCs), are detected with in situ plasma and magnetic measurements. They are the continuation of the CMEs observed with imagers closer to the Sun. A review of their properties is presented with a focus on their magnetic configuration and its evolution. Many recent observations, both in situ and with imagers, point to a key role of flux ropes, a conclusion which is also supported by present coronal eruptive models. Then, is a flux rope generically present in an ICME? How to quantify its 3D physical properties when it is detected locally as a MC? Is it a simple flux rope? How does it evolve in the solar wind? This paper reviews our present answers and limited understanding to these questions.

Keywords. magnetic fields, (magnetohydrodynamics:) MHD, Sun: coronal mass ejections (CMEs), Sun: magnetic fields, interplanetary medium

1. Main characteristics of ICMEs and magnetic clouds

Interplanetary coronal mass ejections (ICMEs) are detected by in situ measurements having unusual characteristics of the solar wind. Depending on authors and available instruments, ICMEs have been defined by a broad set of signatures of the plasma, energetic particles and magnetic field (e.g., see the reviews of Zurbuchen & Richardson 2006; Wimmer-Schweingruber et al. 2006). The main ICME characteristics are summarized in Fig. 1. In the solar wind, the proton temperature is well correlated to its bulk velocity (e.g., Elliott et al. 2005; Démoulin 2009). Then, departure from this law, more precisely where the proton temperature is below half the proton temperature found in the solar wind with the same speed, is a typical definition of an ICME (Liu et al. 2005; Richardson & Cane 2010). ICMEs also have typically enhanced ion charge states which are formed in the corona below the height where the collision rate becomes negligible (see Lepri 2014). ICMEs are also characterized by enhanced abundances of ions with a low first ionisation potential (FIP) compared to those with a high FIP (Fig. 1). This separation of the elements occurs in the low solar atmosphere (e.g., see Baker et al. 2014). All these ICME signatures are typically not present in the same interval of time, they are frequently variable in intensity during an ICME crossing, and even they are not always all present (Richardson & Cane 2010).

Magnetic clouds (MCs) are defined by an enhanced magnetic field strength, a smooth rotation of the magnetic field direction through a large angle and a low proton temperature compare to the expected one in the solar wind (see the reviews of Gosling et al. 1995; Dasso et al. 2005). These local measurements are typically interpreted with a flux rope model (i.e., a twisted magnetic configuration, e.g., Lepping et al. 1990; Lynch et al. 2003; Dasso et al. 2006; Leitner et al. 2007). MCs are present within ICMEs, e.g., Fig. 1. An ICME can coincide with the full time range of the associated MC, be more extended or contain no MC. On average a MC is detected in about 30% of ICMEs (Wu & Lepping 2011). This ratio evolves with the solar cycle from $\approx$ 15% at solar maximum to $\approx$ 100% at solar minimum (Richardson & Cane 2010; Kilpua et al. 2012).

ICMEs are the counterpart of coronal mass ejections (CMEs) observed with coronagraphs

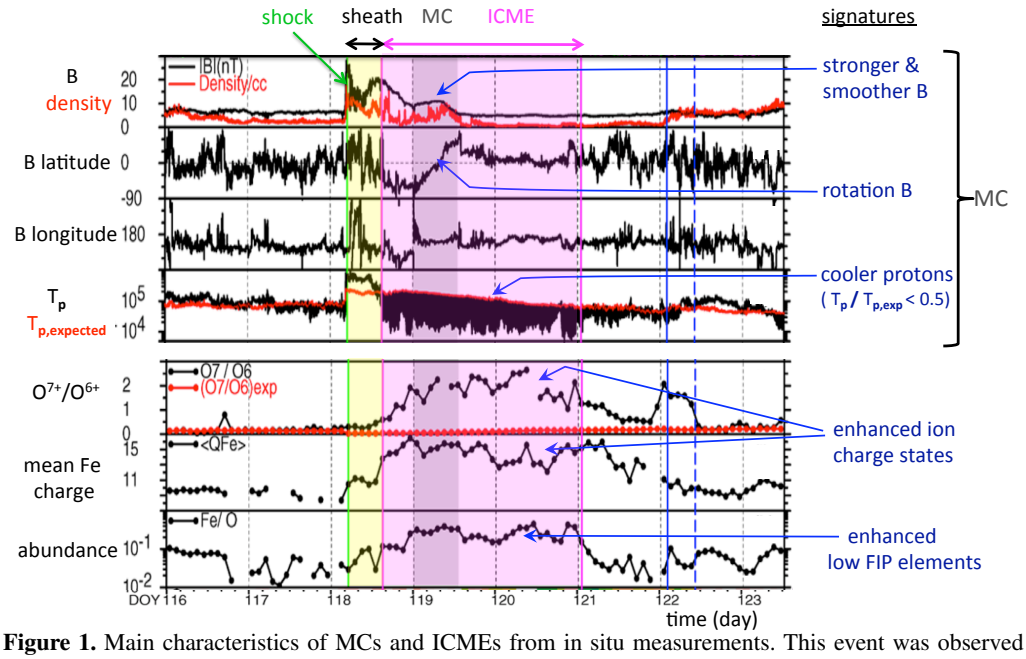

Figure 1. Main characteristics of MCs and ICMEs from in situ measurements. This event was observed from 28 April to 1 May 2001 at 1 AU by ACE spacecraft. A MC is present inside the ICME as shown by the four upper panels. The ICME is defined by the region $T_p < T_{p,expected}/2$ (fourth panel, the region between T_p and $T_{p,expected}$ is set in black inside the ICME). It corresponds approximatively to the regions of enhanced ion charge states and abundance anomaly (lower panels). Adapted from Richardson & Cane (2010).

(e.g., Howard 2011; Lugaz & Roussev 2011). The link between coronal and in situ observations were done by using as many as possible constraint derived by both type of data: the relative location of the solar source and the spacecraft detecting the ICME, the transit time (duration of displacement from the Sun to in situ location), and by the estimation of the same physical parameters (orientation of the magnetic configuration, magnetic fluxes and helicity, see e.g., the review of Démoulin 2007). With STEREO twin spacecraft having both in situ and imager instruments, this link is presently well established (e.g., Harrison et al. 2009; Kilpua et al. 2011; Rouillard 2011; Lugaz et al. 2012, and references therein). An example is shown in Fig. 2 where a CME is followed from its launch in the corona to 1 AU where the ICME/MC was observed by ACE and Wind spacecraft (see Fig. 4 of DeForest et al. 2013). The build up of mass in the sheath by a snowplow effect, as well as the kinetic energy budget were also followed over such a distance.

The solar origin of a CME is the progressive buildup of a flux rope (FR) by magnetic reconnection at a photospheric magnetic inversion line in and also outside active regions, typically where a filament is present. When the magnetic stress is too large, an instability occurs, launching the flux rope (e.g., Török & Kliem 2007; Aulanier et al. 2010). A large amount of the surrounding magnetic arcade is reconnecting below the erupting flux rope, leading to a flare with its two ribbons separating and with the formation of flare loops (see e.g., the review of Schmieder et al. 2013). This process further builds up a very hot FR ($\approx$ 10 MK) as imaged with AIA EUV observations (e.g., Reeves & Golub 2011; Cheng et al. 2011, 2013). Such extreme temperatures are expected to be at the origin of the higher ion charge states in ICMEs (e.g., Gopalswamy et al. 2013). These observations also confirm the global scenario of an eruptive flare leading to a CME (see the reviews of Aulanier 2014; Shibata 2014). Moreover, some specificities of 3D reconnection without magnetic null points, like the continuous slippage of field lines, have been

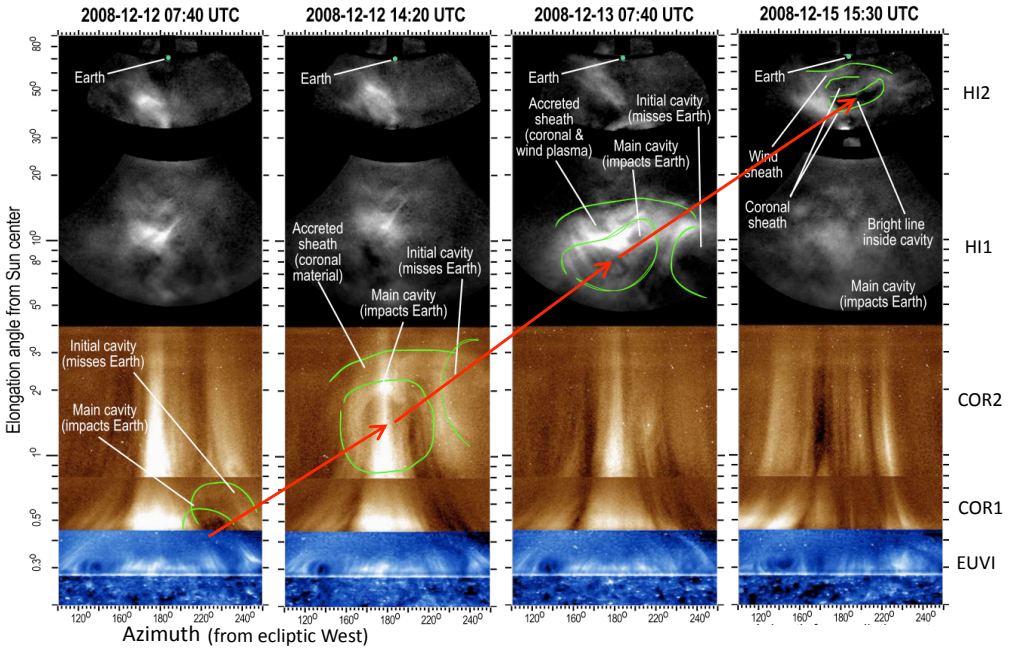

Figure 2. Launch of a CME on December 12, 2008 from the corona and evolution of the associated ICME as observed by the different instruments of STEREO-A (EUVI,COR1,COR2,HI1,HI2). The images have been transformed to the same cylindrical coordinate system (elongation, azimuth). The CME starts by the destabilization of a coronal cavity (plausibly the signature of a flux rope). This cavity is followed all the way to Earth where it is identified as a MC by in situ measurements. Adapted from DeForest et al. (2013).

found in AIA observations and a 3D MHD simulation (Aulanier et al. 2012; Janvier et al. 2013a; Dudik et al. 2014b).

With SDO/AIA observations many clear examples of the formation, then eruption of twisted structures are available (e.g., Title 2014). However, this does not imply that FR signatures are easily observable in all solar events. First, the twist is only just above one turn at the start of an eruption. This weakly twisted FR is even more difficult to visualize when it is bent in a 3D configuration, and even more with typically only very few field lines partially outlined by a sufficiently dense plasma to be emissive enough (it is also very difficult to visualize, from an arbitrary point of view, the 3D configuration involved in MHD simulations with few and partially drawn field lines). More over, background/foreground emissions are typically present, and projection effects should be favorable (e.g., along the FR axis). During the eruption, further twist is built up by reconnection, below the flux rope, of the surrounding arcades. The more potential the arcade is, typically higher up, the more twisted is the resulting wrapping field around the erupting FR (while preserving magnetic helicity). This builds the higher twist observed in situ at the periphery of MCs, but this is typically not observable in EUV images. At the CME stage, it is even more difficult to find evidences of a FR as the scattered light comes mainly from the sheath built up in front of the CME (Fig. 2). This difficulty further increases in the heliospheric imagers as the signal/noise ratio decreases and the interpretation of the images becomes more model dependent (Lugaz 2014). Finally, the in situ observations only provide a 1D cut through a 3D evolving magnetic configuration, so modeling and interpretation are required. In brief, in order to detect the FR within an erupting configuration, a CME or an ICME, the Sun must “cooperate” with us!

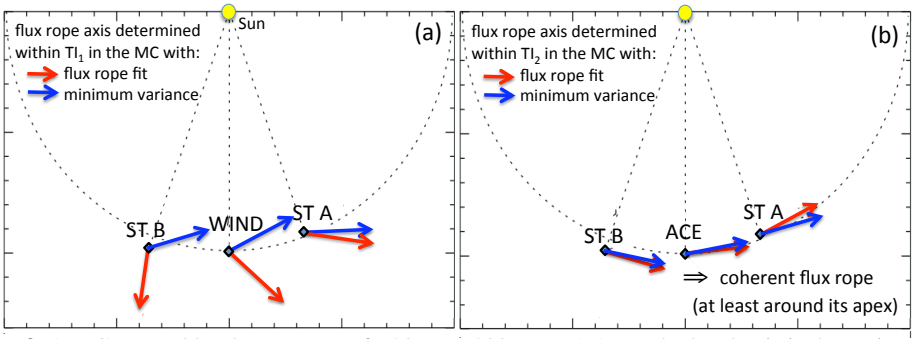

Figure 3. A MC crossed by three spacecraft (20 Nov. 2007 at ≈ 1 AU). The local axis is determined from a minimum variance (MV) or a fit of a Lundquist's model to the in situ $\vec{B}$ data. The methods are applied to two different Time Intervals (TI) within the MC. While the MV and the fit techniques significantly disagree in (a), they give comparable directions in (b) and moreover a coherent global shape of the MC axis. Adapted respectively from Farrugia et al. (2011) and Ruffenach et al. (2012).

2. Structure and evolution of magnetic clouds

Since in situ data are typically available only along the 1D crossing of some MCs by one spacecraft, a magnetic model is needed to derive, at least around the trajectory, the magnetic configuration. A FR model is typically due to the smooth rotation of the magnetic field across a MC, as well as the relationship with erupting twisted configurations on the Sun. Its free parameters are determined by a least square fit to the in situ data. So far, no model has been proven to best represent a large set of MCs. Many models consider a straight FR as a local approximation. The simplest and most used model is a linear force-free field model, called Lundquist's model (see e.g. Lepping et al. 1990; Leitner et al. 2007). Extensions to non circular cross-section (e.g. Vandas & Romashets 2003; Démoulin & Dasso 2009b), or non force-free models (e.g. Mulligan & Russell 2001; Hidalgo 2011) have been developed. An alternative is to solve magneto-hydrostatic equations, which reduce to the Grad-Shafranov equation with an axis of invariance, together with the observed boundary conditions for the integration procedure (e.g., Isavnin et al. 2011; Hu & Qiu 2014).

An appealing approach is to extend the above models to toroidal geometry in order to include the curvature of the FR axis as in the schema of Fig. 5a (e.g. Marubashi & Lepping 2007; Romashets & Vandas 2009). This is especially needed when the spacecraft is crossing one MC leg as the spacecraft explores only a fraction of the FR (e.g. Marubashi et al. 2012; Owens et al. 2012). However, toroidal models imply a larger number of free parameters and it is not yet clear if they can all be constrained by the data of a single spacecraft, even for a MC crossing with a low impact parameter (distance of the spacecraft to the MC axis normalized by its radius). Two well separated spacecraft provide more constraints to the toroidal model (Nakagawa & Matsuoka 2010). However, the number of MCs observed is very limited in this configuration as it requires a FR close to the ecliptic where spacecraft are typically located (see the review of Kilpua et al. 2011).

The simplest way for estimating the FR orientation is to apply the Minimum Variance (MV) method to the normalized series of magnetic field measurements within the MC (e.g., Lepping et al. 1990). It provides a good orientation (with a bias lower than 20°) if the MC is not too asymmetric and the boundaries are well defined (i.e., includes only the flux rope, Gulisano et al. 2007). A fit of a model, like Lundquist's, to the data also provides an estimation of the local axis direction. Both methods, and others, can provide very different orientations if they are applied to different ICMEs boundaries while a better agreement is found with the same boundaries (Al-Haddad et al. 2013). For example, MV and FR fit methods give significant different orientations, and moreover without coherence along the MC when the time intervals TI_1 are used at the

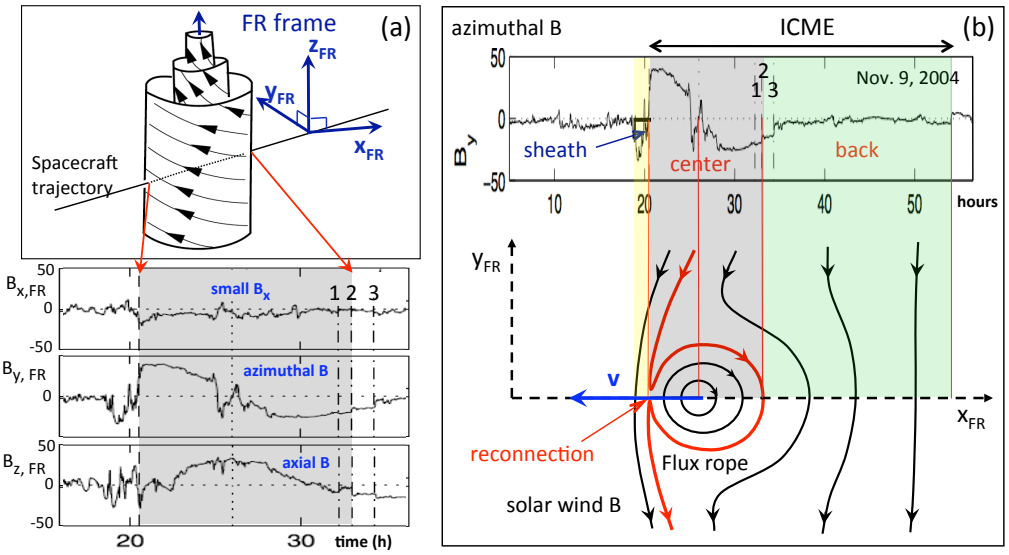

Figure 4. Definition of the flux rope (FR) frame and MC back region. **(a)** Schema of a FR and its associated local frame. Below, an example of observed magnetic field (9 Nov. 2004 at 1 AU) in the FR frame. This MC was crossed by a spacecraft close to the FR axis (small $< B_x > / < B >$ value). The numbers 1,2,3 show possible rear boundaries associated to discontinuities of $\vec{B}$. The azimuthal flux balance identifies the rear boundary as the number 2. **(b)** Extended time interval of the same MC which extends up to $t \approx 55$ h. At the time of the spacecraft crossing, the FR is limited to the grey region, while a long back region (green region) is present with a mix of MC and solar wind characteristics. This back region was part of the FR closer to the Sun before reconnection arround the FR front occurred (bottom schema and Fig. 5). Adapted from Dasso et al. (2007).

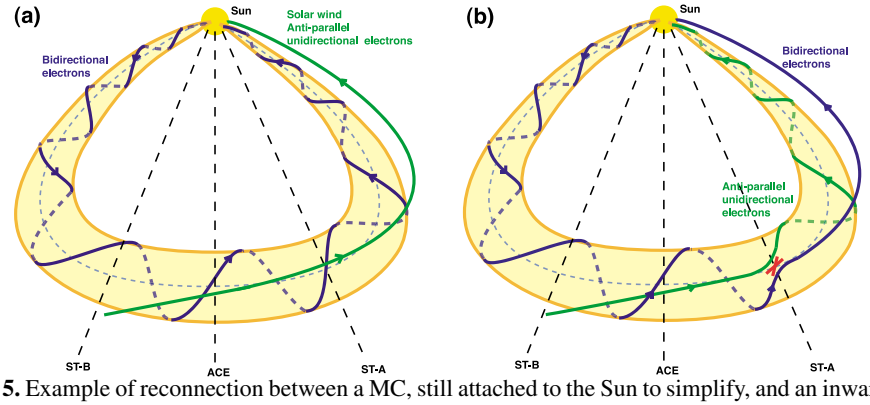

Figure 5. Example of reconnection between a MC, still attached to the Sun to simplify, and an inward sector magnetic field. **(a)** Before reconnection. **(b)** Part of the magnetic flux is removed from the MC front around the reconnection region (by shifting on the FR sides) creating a back region (Fig. 4). However, the in situ detection of this process depends on the location of the spacecraft crossing (here a back is present at ST-A, but not at ST-B and ACE). Adapted from Ruffenach et al. (2012).

three spacecraft (Fig. 3a, Farrugia et al. 2011), while they give consistent results when the time intervals TI_2 are rather used (Fig. 3b, Ruffenach et al. 2012).

A MC travels typically at a different speed than the surrounding solar wind, then their respective magnetic fields are pushed together, generally implying magnetic reconnection. This leads to a FR progressively peeling off layers until only the central region remains as a coherent FR when crossed by a spacecraft (Dasso et al. 2006). Figures 4 and 5 illustrate two MCs where reconnection happened in the front leaving a back region behind the remaining FR. This region

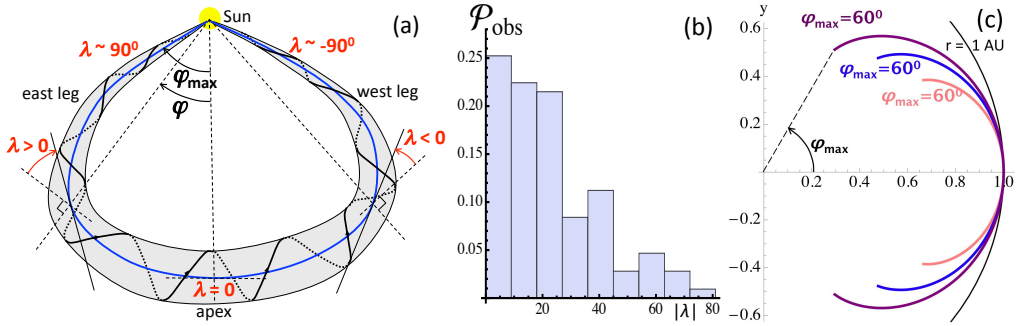

Figure 6. Statistical determination of the mean MC axis shape from a set of MCs observed at 1 AU. **(a)** Schema of a FR and definition of the location angle λ (angle between the local axis direction and the ortho-radial from the Sun), **(b)** Distribution of $|\lambda|$ as observed at 1 AU for 107 MCs (Lepping & Wu 2010). **(c)** Shape of the mean MC axis deduced from (b), with the maximum angular extension, φ_{max}, as the only free parameter. Adapted from Janvier et al. (2013b).

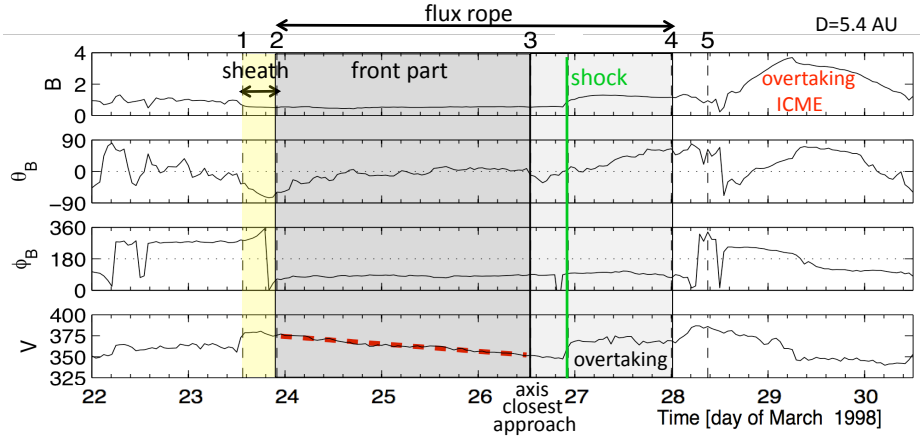

Figure 7. Example of a MC strongly overtaken by an ICME when observed by Ulysses at 5.4 AU. Only the first part, before the FR axis, is unperturbed (dark grey region) while the second part is strongly compressed and deformed (light grey region). The same MC was observed at 1 AU by ACE when it was not yet overtaken. Its magnetic field was similar to the MC in Fig. 4, with a smaller back region ($\approx 1/5$ of the FR extension). Adapted from Nakwacki et al. (2011).

has mixed properties between MC and solar wind ones. The leading edge of the back region was determined by the azimuthal flux balance. This was confirmed by the presence of a magnetic discontinuity (Dasso et al. 2007; Nakwacki et al. 2011) as well as by in situ reconnection signatures (Ruffenach et al. 2012). Finally, the FR orientation, determined, e.g., by an MV or a FR fit, can be significantly biased if the method is applied to the full MC time interval. Then, it is important to define the MC boundaries in order to have a balance of the azimuthal magnetic flux before and after the closest approach to the FR axis (Fig. 4b). This is achieved in the FR frame (Fig. 4a), and it removes the back region from the time interval selected to apply an MV or a FR fit (Dasso et al. 2006, 2007).

While few MCs have been observed by at least two spacecraft with a low impact parameter, more than one hundred MCs have been observed by Wind spacecraft and fitted by the Lundquist model (Lepping & Wu 2010). The inclination of the FR axis on the ortho-radial direction defines the angle λ which is related to the location of the spacecraft crossing along the FR axis (Fig. 6a). From the distribution of λ (Fig. 6b), Janvier et al. (2013b) showed that one can derive a mean axis shape (Fig. 6c). It depends only on one free parameter, φ_{max}, which can be constrained from heliospheric imagers (as on STEREO) in favorable cases (Janvier et al. 2014). The mean derived axis shape (Fig. 6c) is compatible with the MC observed by three spacecraft (Fig. 3b).

Apart from reconnection, MCs are also evolving as they move away from the Sun. In particular they are expanding since the surrounding total pressure decreases rapidly with the distance (as $\approx D_{\odot}^{-2.9\pm0.3}$ where $D_{\odot}$ is the distance to the Sun, Démoulin & Dasso 2009a; Gulisano et al. 2010). This expansion is detected in situ by a faster velocity in front than at the rear of the MC, with typically a linear profile (see the V panel of Fig. 7). Démoulin et al. (2008) quantifies this expansion with an nondimensional parameter called ζ which can be derived from in situ measurements. When ζ is constant, the FR radius evolves with $D_{\odot}$ as $R \propto D_{\odot}^{\zeta}$. From observations of different MCs at significantly different helio-distances (Wang et al. 2005; Leitner et al. 2007) and from observations of the velocity profile slope from single spacecraft observations (Démoulin et al. 2008; Gulisano et al. 2010, 2012), from the inner heliosphere to 5 AU, it has been found that $\zeta \approx 0.9 \pm 0.3$ for MCs which are not perturbed (e.g., not overtaken by a fast stream or ICME). In particular, one MC was observed both at 1 AU and 5.4 AU by ACE and Ulysses spacecraft, and indeed $\zeta \approx 0.7$ at both distances (only the front part is used at 5.4 AU because the part of the MC after its axis was strongly distorted by the overtaken ICME, Fig. 7). It implies an expansion by a factor ≈ 3.5. From a fit of the Lundquist model and also from a direct integration of the data of the front part, assuming cylindrical symmetry, Nakwacki et al. (2011) estimated the magnetic fluxes, helicity and energy. They showed that fluxes and helicity were well conserved while magnetic energy decayed almost as expected (as $\approx D_{\odot}^{-\zeta}$).

3. Are MC and non-MC ICMEs different types of events?

The observed magnetic field in MCs is typically modeled by FRs (Sect. 2), but only about one third of ICMEs have a detected MC inside (Sect. 1). Then, are non-MC ICMEs formed by the simple blowout of magnetic arcades from the Sun, so without FR (Gosling 1990), or rather do the spacecraft miss it? Even more, does a MC necessarily include a FR? Al-Haddad et al. (2011) rather proposed the eruption of a strongly sheared (not writhed) arcade to explain the coherent rotation of the magnetic field in MCs. They further argue that magnetic reconstruction methods, such as the Grad-Shafranov one, are biased to recover a FR even when the analyzed field is only a sheared arcade. However, they numerically simulate only very broad cases (almost as broad as the solar distance) and it is difficult to imagine how such model can explain typical MCs, with a radius of 0.1 AU at 1 AU, and even more the smaller ones. Moreover, there is presently no model which blows up an arcade from the Sun without non-physical numerical forcing (Aulanier 2014).

Could spacecraft miss the FR in many events as argued by Jian et al. (2006) from an analysis of the total (almost) pressure profile? Indeed, some MCs have a modest rotation of the magnetic field (down to $\approx 40°$, Lepping & Wu 2010). This is more an observing bias than an intrinsic difference of twist amount, as they are almost equally well fitted by a Lundquist model. Although MCs are expected to be crossed at random positions by a spacecraft, leading to a flat distribution of the impact parameter, the observed probability distribution of the impact parameter actually shows a strongly decreasing function (Lepping & Wu 2010). Does this imply that many MCs, with a moderate or large impact parameter, are not recognized as MCs? This would explain why only one third of ICMEs have a MC inside. However, a quantitative analysis shows that this bias has a small effect; rather the impact parameter distribution is naturally explained by an oblateness of the MC cross section which is elongated by a factor 2 to 3 in the direction perpendicular to the radial from the Sun (Démoulin et al. 2013), in global agreement with other estimations (e.g., Antoniadou et al. 2008; Savani et al. 2010) and magnetohydrodynamics simulations (e.g., Lugaz et al. 2005; Xiong et al. 2006).

Two workshops were organized in order to further investigate the possible difference between MC and non-MC ICMEs. Shock-driven ICMEs observed at 1 AU were selected in the time period 1996-2006. Only the ICMEs with an identified solar source within a longitude range $\pm 15^0$ were selected which reduced the number of ICMEs to 54 events. If the CMEs are FRs launched radially

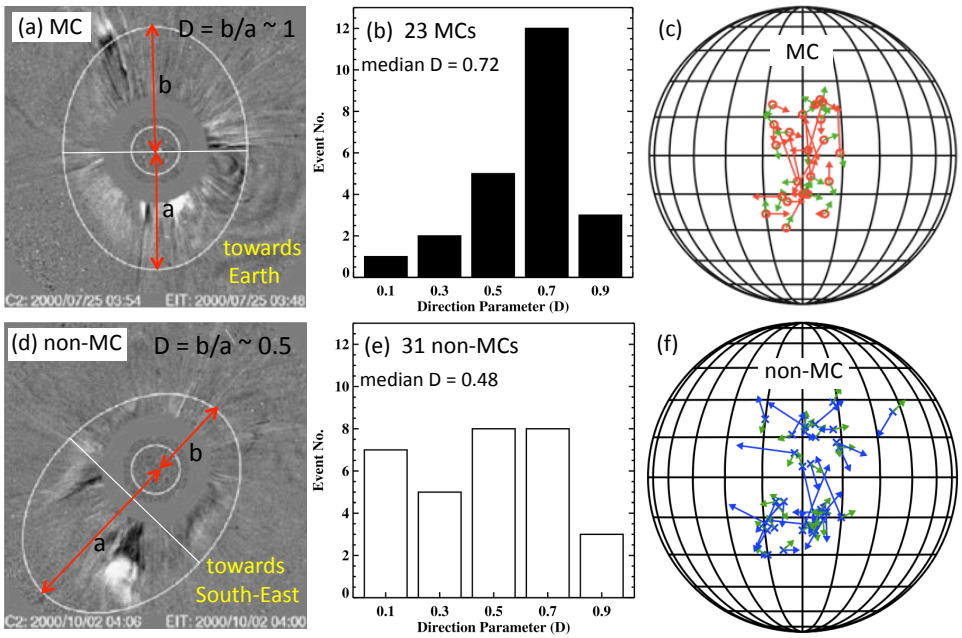

Figure 8. Deflection of CMEs by coronal holes. All CMEs start close to the central meridian (right panels). CMEs are detected close to Earth as MCs (a-c) and non-MC ICMEs (d-f). **(a,d)** The CME direction is estimated by the ratio $D = b/a$ of an ellipse fitted by eyes to the CME front observed by SoHO/LASCO. **(b,e)** Distributions of D showing that CMEs associated to a MC have larger D values, so are more Earth directed, than non-MC CMEs. **(c,f)** Amount of CME deflection from the CME source location towards its propagation direction in the outer coronagraph (red and blue arrows). The green arrows are for a model of coronal hole deflection. Adapted from Yashiro et al. (2013), Kim et al. (2013), and Mäkelä et al. (2013).

from the Sun, a large proportion of MCs is expected to be detected near Earth. However, only 23 MCs were detected. Does it imply that the 31 non-MC ICMEs have no FR, so that a different erupting configuration is present on the Sun? In fact no significant difference was found between the flare temperature, the flare loop properties (size, duration, tilt) as well as the latitude and longitude of the source regions between the two groups (MC and non-MC ICMEs, Gopalswamy et al. 2013; Yashiro et al. 2013). The main difference was the flare magnitude, the median being M1.5 and C4.1 for MC and non-MC ICMEs, respectively, while the distributions were broad and largely overlapped.

The next step was to compare the CME properties. Again no significant difference between the two groups was found for the CME velocity, acceleration and angular width (all projected in the plan of sky, Gopalswamy et al. 2013; Xie et al. 2013). However, a significant difference was found in the CME propagation direction estimated by fitting visually the CME front with an ellipse (Kim et al. 2013; Zhang et al. 2013). More precisely, they analyzed the direction parameter, D (Fig. 8a,d), and found that the CMEs associated to MCs are more directed towards the observing spacecraft than the ones associated to non-MC ICMEs (Fig. 8b,e). This result is confirmed by fitting visually the CME front with a flux-rope like model (Xie et al. 2013). Moreover, Mäkelä et al. (2013) confirmed that CMEs are deflected by the magnetic field of coronal holes as found in MHD simulations (e.g. Lugaz et al. 2011). The deflection is stronger with a closer coronal hole with larger magnetic flux, as expected. The key point is that CMEs associated to MCs are deviated towards the spacecraft direction, while the ones associated to non-MC ICMEs are deflected away (Fig. 8d,f). The main conclusion of all these papers is that the difference between MC and non-MC ICMEs is a selection effect, and not an intrinsic property of the solar source or of the ejected configuration, in agreement with Jian et al. (2006).

4. Overview

There is a broad range of observations and models which are pointing towards a key role of flux ropes (FRs) in the corona, CMEs and ICMEs as follows. Well before an eruption, the presence of magnetic dips, then of a twisted field in bipolar configurations, is needed to support the dense plasma of filaments (Dudik et al. 2014a). The structure of coronal cavities is also naturally explained by the presence of a FR (Gibson 2014). Next, an evolution from an arcade to a sigmoid is typically observed in EUV and X-rays before and during eruptions (Green 2014). The main mechanism of eruption is thought to be the loss of equilibrium / torus instability which involves a FR (Aulanier 2014; Olmedo & Zhang 2014). In some eruption, the kink instability of a FR could also play a role. Finally, in situ data of MCs are compatible with a FR configuration (Sect. 2) and all evidences point toward the conclusion that ICMEs should all contain FRs (Sect. 3).

All these FR evidences are remarkable taking into account the difficulties in observing 3D FRs with both imagers and in situ data. Further, the FRs are initially embedded in complex 3D coronal magnetic configurations and they reconnect with the surrounding encountered fields as they propagate, creating a back region (e.g., Ruffenach et al. 2012). It is important to well define the FR boundaries before fitting a model to the in situ data in order to derive more global quantities. To further progress on the magnetic configuration involved, we need to combine the analyze of some clear events with multi-instruments and spacecraft (e.g. Möstl et al. 2009), with statistical studies (e.g. Janvier et al. 2013b) and with numerical simulations (as reviewed by Lugaz 2014).

Acknowledgements. I thank Sergio Dasso, Miho Janvier, Alexis Ruffenach, and David Webb for useful comments.

References

Al-Haddad, N., Nieves-Chinchilla, T., Savani, N., et al. 2013, *Solar Phys.*, 284, 129
Al-Haddad, N., Roussev, I. I., Möstl, C., et al. 2011, *ApJL*, 738, L18
Antoniadou, I., Geranios, A., Vandas, M., et al. 2008, *Planet. Spa. Sci.*, 56, 492
Aulanier, G. 2014, IAUS 300, this issue
Aulanier, G., Janvier, M., & Schmieder, B. 2012, *A&A*, 543, A110
Aulanier, G., Török, T., Démoulin, P., & DeLuca, E. E. 2010, *ApJ*, 708, 314
Baker, D., Brooks, D., Démoulin, P., et al. 2014, IAUS 300, this issue
Cheng, X., Zhang, J., Ding, M. D., et al. 2013, *ApJL*, 769, L25
Cheng, X., Zhang, J., Liu, Y., & Ding, M. D. 2011, *ApJL*, 732, L25
Dasso, S., Mandrini, C. H., Démoulin, P., & Luoni, M. L. 2006, *A&A*, 455, 349
Dasso, S., Mandrini, C. H., Démoulin, P., Luoni, M. L., & Gulisano, A. M. 2005, *Adv. Spa. Res.*, 35, 711
Dasso, S., Nakwacki, M. S., Démoulin, P., & Mandrini, C. H. 2007, *Solar Phys.*, 244, 115
DeForest, C. E., Howard, T. A., & McComas, D. J. 2013, *ApJ*, 769, 43
Démoulin, P. 2007, *Ann. Geophys.*, 26, 3113
Démoulin, P. 2009, *Solar Phys.*, 257, 169
Démoulin, P. & Dasso, S. 2009a, *A&A*, 498, 551
Démoulin, P. & Dasso, S. 2009b, *A&A*, 507, 969
Démoulin, P., Dasso, S., & Janvier, M. 2013, *A&A*, 550, A3
Démoulin, P., Nakwacki, M. S., Dasso, S., & Mandrini, C. H. 2008, *Solar Phys.*, 250, 347
Dudik, J., Aulanier, G., Schmieder, B., Zapior, M., & Heinzel, P. 2014a, IAUS 300, this issue
Dudik, J., Janvier, M., Del Zanna, G., et al. 2014b, IAUS 300, this issue
Elliott, H. A., McComas, D. J., Schwadron, N. A., et al. 2005, *JGR*, 110, A04103
Farrugia, C. J., Berdichevsky, D. B., Möstl, C., et al. 2011, *JASTP*, 73, 1254
Gibson, S. 2014, IAUS 300, this issue
Gopalswamy, N., Mäkelä, P., Akiyama, S., et al. 2013, *Solar Phys.*, 284, 17
Gosling, J. T. 1990, In Physics of magnetic flux ropes, American Geophysical Union, 58, 343
Gosling, J. T., Bame, S. J., McComas, D. J., et al. 1995, *Space Sci. Revs*, 72, 133
Green, L. 2014, IAUS 300, this issue

Gulisano, A. M., Dasso, S., Mandrini, C. H., & Démoulin, P. 2007, *Adv. Spa. Res.*, 40, 1881
Gulisano, A. M., Démoulin, P., Dasso, S., & Rodriguez, L. 2012, *A&A*, 543, A107
Gulisano, A. M., Démoulin, P., Dasso, S., Ruiz, M. E., & Marsch, E. 2010, *A&A*, 509, A39
Harrison, R. A., Davies, J. A., Rouillard, A. P., et al. 2009, *Solar Phys.*, 256, 219
Hidalgo, M. A. 2011, *JGR*, 116, 2101
Howard, T. A. 2011, *JASTP*, 73, 1242
Hu, Q. & Qiu, J. 2014, IAUS 300, this issue
Isavnin, A., Kilpua, E. K. J., & Koskinen, H. E. J. 2011, *Solar Phys.*, 273, 205
Janvier, M., Aulanier, G., Pariat, E., & Démoulin, P. 2013a, *A&A*, 555, A77
Janvier, M., Démoulin, P., & Dasso, S. 2013b, *A&A*, 556, A50
Janvier, M., Démoulin, P., & Dasso, S. 2014, IAUS 300, this issue
Jian, L., Russell, C. T., Luhmann, J. G., & Skoug, R. M. 2006, *Solar Phys.*, 239, 393
Kilpua, E. K. J., Jian, L. K., Li, Y., & et al. 2011, *JASTP*, 73, 1228
Kilpua, E. K. J., Jian, L. K., Li, Y., Luhmann, J. G., & Russell, C. T. 2012, *Solar Phys.*, 56
Kim, R.-S., Gopalswamy, N., Cho, K.-S., Moon, Y.-J., & Yashiro, S. 2013, *Solar Phys.*, 284, 77
Leitner, M., Farrugia, C. J., Möstl, C., et al. 2007, *JGR*, 112, A06113
Lepping, R. P., Burlaga, L. F., & Jones, J. A. 1990, *JGR*, 95, 11957
Lepping, R. P. & Wu, C. C. 2010, *Ann. Geophys.*, 28, 1539
Lepri, S. 2014, IAUS 300, this issue
Liu, Y., Richardson, J. D., & Belcher, J. W. 2005, *Planet. Spa. Sci.*, 53, 3
Lugaz, N. 2014, IAUS 300, this issue
Lugaz, N., Downs, C., Shibata, K., et al. 2011, *ApJ*, 738, 127
Lugaz, N., Kintner, P., Möstl, C., et al. 2012, *Solar Phys.*, 279, 497
Lugaz, N., Manchester, IV, W. B., & Gombosi, T. I. 2005, *ApJ*, 627, 1019
Lugaz, N. & Roussev, I. 2011, *JASTP*, 73, 1187
Lynch, B. J., Zurbuchen, T. H., Fisk, L. A., & Antiochos, S. K. 2003, *JGR*, 108, A01239
Mäkelä, P., Gopalswamy, N., Xie, H., et al. 2013, *Solar Phys.*, 284, 59
Marubashi, K., Cho, K.-S., Kim, Y.-H., Park, Y.-D., & Park, S.-H. 2012, *JGR*, 117, 1101
Marubashi, K. & Lepping, R. P. 2007, *Ann. Geophys.*, 25, 2453
Möstl, C., Farrugia, C. J., Temmer, M., et al. 2009, *ApJL*, 705, L180
Mulligan, T. & Russell, C. T. 2001, *JGR*, 106, 10581
Nakagawa, T. & Matsuoka, A. 2010, *JGR*, 115, 10113
Nakwacki, M., Dasso, S., Démoulin, P., & et al. 2011, *A&A*, 535, A52
Olmedo, O. & Zhang, J. 2014, IAUS 300, this issue
Owens, M. J., Démoulin, P., Savani, N. P., Lavraud, B., & Ruffenach, A. 2012, *Solar Phys.*, 278, 435
Reeves, K. K. & Golub, L. 2011, *ApJL*, 727, L52
Richardson, I. G. & Cane, H. V. 2010, *Solar Phys.*, 264, 189
Romashets, E. & Vandas, M. 2009, *A&A*, 499, 17
Rouillard, A. P. 2011, *JASTP*, 73, 1201
Ruffenach, A., Lavraud, B., Owens, M. J., et al. 2012, *JGR*, 117, A09101
Savani, N. P., Owens, M. J., Rouillard, A. P., & et al. 2010, *ApJL*, 714, L128
Schmieder, B., Démoulin, P., & Aulanier, G. 2013, *Adv. Spa. Res.*, 51, 1967
Shibata, S. 2014, IAUS 300, this issue
Title, A. 2014, IAUS 300, this issue
Török, T. & Kliem, B. 2007, Astronomische Nachrichten, 328, 743
Vandas, M. & Romashets, E. P. 2003, *A&A*, 398, 801
Wang, C., Du, D., & Richardson, J. D. 2005, *JGR*, 110, A10107
Wimmer-Schweingruber, R. F., Crooker, N. U., Balogh, A., et al. 2006, *Space Sci. Revs*, 123, 177
Wu, C.-C. & Lepping, R. P. 2011, *Solar Phys.*, 269, 141
Xie, H., Gopalswamy, N., & St. Cyr, O. C. 2013, *Solar Phys.*, 284, 47
Xiong, M., Zheng, H., Wang, Y., & Wang, S. 2006, *JGR*, 111, A08105
Yashiro, S., Gopalswamy, N., Mäkelä, P., & Akiyama, S. 2013, *Solar Phys.*, 284, 5
Zhang, J., Hess, P., & Poomvises, W. 2013, *Solar Phys.*, 284, 89
Zurbuchen, T. H. & Richardson, I. G. 2006, *Space Sci. Revs*, 123, 31